Geoderma 467 (2026) 117734

Contents lists available at ScienceDirect

Geoderma

journal homepage: www.elsevier.com/locate/geoderma

Maize root growth, oxygen and N availability drive formation of N_2O hotspots in soil

Pauline Sophie Rummel [a,b,c,**], Martin Reinhard Rasmussen [a,d], Aurélien Saghaï [e], Theresa Merl [a], Sara Hallin [e], Carsten W. Mueller [b,f], Klaus Koren [a,*]

[a] Aarhus University, Department of Biology, Section for Microbiology, Aarhus, Denmark
[b] University of Copenhagen, Department of Geosciences and Natural Resource Management, Geography, Copenhagen, Denmark
[c] Hasselt University, Centre for Environmental Sciences, Hasselt, Belgium
[d] Aarhus University, Center for Landscape Research in Sustainable Agricultural Futures, Aarhus, Denmark
[e] Swedish University of Agricultural Sciences, Department of Forest Mycology and Plant Pathology, Uppsala, Sweden
[f] Technische Universität Berlin, Institute of Ecology, Chair of Soil Science, Berlin, Germany

ARTICLE INFO

Handling Editor: Dr Mariluz Cayuela

Keywords:
Denitrification
Rhizosphere
Planar optodes
Microsensors
qPCR

ABSTRACT

Plant roots can modify all major controls of denitrification in soils, particularly the availability of the main substrates (NO_3^- and C_{org}), soil moisture, soil O_2 content, and root-associated microbial communities, and thus play an important role in N_2O formation. Direct *in-situ* measurements of N_2O concentrations in the rhizosphere are lacking, yet are crucial to better understand how rhizosphere denitrification contributes to overall N_2O emissions from soil. We equipped rhizoboxes with O_2-sensitive planar optodes to simultaneously monitor root growth and rhizosphere/soil O_2 concentrations. We measured soil surface N_2O fluxes and linked them to root growth, soil moisture, and root/soil O_2 concentrations. Based on root growth and O_2 concentrations, we identified regions of interest (ROI) and sampled small soil volumes, which were analyzed for C and N content, and abundance of genes indicative of microbial denitrifiers (*nirK*, *nirS*) and N_2O reducers (*nosZ*I, *nosZ*II), and soil N_2O concentrations. Plant roots determined depth gradients of nutrients and denitrification gene abundances in the soil of the rhizoboxes with higher resource availability (NO_3^-, DOC) and lower soil moisture in the upper soil layers, which also had higher abundances of total bacteria, *nirK* and *nosZ*II. These findings indicate that the uppermost soil layers largely contributed to N_2O formation. Our study provides the first direct evidence of roots creating distinct O_2 and N gradients controlling N_2O production at the process scale leading to high *in-situ* N_2O concentrations.

1. Introduction

Plant roots play an important role in regulating denitrification, the main process contributing to the formation of the climate-relevant greenhouse gas nitrous oxide (N_2O) (Butterbach-Bahl et al., 2013; Ciais et al., 2013). Denitrification is the sequential reduction of nitrate (NO_3^-) to nitrite (NO_2^-), nitric oxide (NO), nitrous oxide (N_2O), and molecular nitrogen (N_2) by heterotrophic bacteria, fungi, and archaea (Zumft, 1997). Plant roots modify major controls on denitrification by altering soil moisture, O_2 content, the availability of the main substrates (NO_3^- and C_{org}), and root-associated microbial communities. Although plant and root effects on denitrification are well studied, direct in-situ measurements of N_2O concentrations in the rhizosphere are scarce. Yet, disentangling the factors that drive N_2O formation in microsites is crucial for understanding N_2O emissions and to develop mitigation strategies.

Increased N_2O losses have been reported from planted compared to bare soils (Woldendorp, 1963; Vinther, 1984; Senbayram et al., 2020; Yankelzon et al., 2024) and the promoting effect of plant growth on denitrification has been associated with higher C_{org} availability in the rhizosphere (Smith & Tiedje, 1979; Bakken, 1988; Philippot et al., 2009), and the soil volume directly affected by plant root activity (Lambers et al., 2009). Plants translocate 20–30 % of assimilated C belowground and about 7–11 % of assimilated C enters the soil as

* Corresponding author.
** Corresponding author at: Hasselt University, Centre for Environmental Sciences, Hasselt, Belgium.
E-mail addresses: pauline.rummel@uhasselt.be (P.S. Rummel), klaus.koren@bio.au.dk (K. Koren).

https://doi.org/10.1016/j.geoderma.2026.117734
Received 28 October 2025; Received in revised form 5 February 2026; Accepted 9 February 2026
Available online 14 February 2026

rhizodeposition (Pausch & Kuzyakov, 2018). Higher C availability in the rhizosphere attracts soil microorganisms including bacteria, fungi, oomycetes, and archaea feeding on rhizodeposits, making the rhizosphere a hotspot of microbial activity (Starkey, 1958; Philippot et al., 2013). In addition to microbial respiration, root respiration largely contributes to O_2 consumption in soil with rates of around 20 mg O_2 m^{-1} root d^{-1} for maize roots (Ben-Noah & Friedman, 2018). Root and microbial respiration decrease O_2 availability in the rhizosphere, creating suitable conditions for denitrification (Bateman & Baggs, 2005; Hu et al., 2015, Lacroix et al., 2025). Accordingly, denitrifiers are more abundant in the rhizosphere than the bulk soil of a range of different plant species (Knowles, 1982; Chèneby et al., 2004; Ai et al., 2020; Wang et al., 2024). Nitrate reduction and denitrification activities are reportedly higher in rhizosphere soil compared to bulk soil (Smith & Tiedje, 1979; Klemedtsson et al., 1987; Bakken, 1988; Mahmood et al., 1997; Hamonts et al., 2013; Guyonnet et al., 2017; Malique et al., 2019; Zhao et al., 2020).

Direct in-situ measurements of N_2O concentrations in the rhizosphere are lacking, yet crucial to understanding how roots control denitrification and N_2O formation. Further, it remains unknown to what extent rhizosphere denitrification contributes to overall N_2O emissions from soil and how microscale N_2O production relates to surface N_2O fluxes. Denitrification takes place in microbial hotspots – small soil volumes with faster process rates compared to the average soil conditions (=cold spots) (Groffman et al., 2009; Kuzyakov & Blagodatskaya, 2015). Characterization of these N_2O hot and cold spots is needed to better understand the 'rhizosphere effect' and its significance for N_2O emissions.

This study aimed to (I) elucidate how plant roots control formation of N_2O hotspots in the rhizosphere, (II) determine spatial distribution of N_2O concentrations in relation to root growth and development, and (III) characterize genetic potential for microbial N cycling in N_2O hot and cold spots. We hypothesize that (I) N_2O fluxes from soil increase with increasing root growth, (II) increased microbial respiration in the rhizosphere stimulates formation of N_2O hotspots in close proximity to the roots, and (III) N_2O hotspots are characterized by higher availability of C and N, and higher abundance of denitrifying and N_2O reducing microorganisms compared to cold spots with low N_2O concentrations. To address these hypotheses, we equipped rhizoboxes with O_2-sensitive planar optodes to simultaneously monitor root growth and rhizosphere/soil O_2 concentrations. We further measured surface N_2O fluxes and linked them to root growth, soil moisture, and root/soil O_2 concentrations. Finally, we defined regions of interest (ROI) based on root growth and O_2 concentrations, and analyzed them for C, N, abundance of microbial N reducers, and soil N_2O concentrations.

2. Material and methods

2.1. Rhizobox setup

2.1.1. Optode fabrication

Planar optodes are a non-invasive imaging technique based on reversible changes in luminescence properties of analyte-specific fluorophores enabling visualization and quantification of biochemical processes with an emphasis on capturing spatial and temporal heterogeneity (Blossfeld, 2013). The O_2 optodes were prepared as previously described by Merl & Koren (2020): 76.5 mg of the indicator dye PtTFPP (Platinum(II)-meso(2,3,4,5,6-pentafluoro)phenyl-porphyrin, Frontier Scientific, Newark, USA), 76.8 mg of the reference dye MY (Macrolex® fluorescence yellow 10GN, Lanxess, Köln, Germany), and 5 g Polystyrene (Sigma Aldrich, Burlington, USA) were dissolved in 50 g Toluene. This 'sensor cocktail' was knife-coated onto a PET foil (Optimont® 501, Bleher Folientechnik GmbH, Ditzingen-Heimerdingen, Germany) using a film applicator (BYK, Wesel, Germany) and a layer of ~ 10 μm was obtained after the toluene evaporated.

2.1.2. Soil

The soil was collected from a long-term experimental field site in Rotthalmünster, Germany (N48°21′, E13°11′). It was characterized a Haplic Luvisol (according to IUSS Working Group WRB, 2022) with a silty loamy texture (19 % clay, 71 % silt, 10 % sand), a pH ($CaCl_2$) of 6.74, with 0.13 % $CaCO_3$. The soil organic carbon content was 1.21 %, total soil nitrogen was 0.14 %, and the C:N ratio was 8.65. Soil was air-dried, sieved to 10 mm mesh size, and stored at 4 °C until the beginning of the experiment.

2.1.3. Experimental setup

The experiment was conducted in rhizoboxes with inner dimensions of 20 cm x 2.2 cm x 40 cm (width x depth x height). Each box had three holes (7 mm diameter) in the bottom part allowing for drainage. The inner sides were lined with a polyester wick (Breatex™ 150, Fibertex Nonwovens A/S, Aalborg, Denmark) facilitating rewetting and soil moisture distribution. The "window side" of the rhizoboxes consisted of an opaque frame and transparent, removable acrylic glass windows (Linatex A/S, Herlev, Denmark) (Fig. 1). The O_2 optode was adhered onto the grid at the window side of the rhizoboxes with insulation tape. Rhizoboxes were closed using a rubber seal and C-clamps.

Dry soil was mixed with finely ground fertilizer (Pioner NPK Makro BLÅ, Azelis A/S, Kgs. Lyngby, Denmark) supplying 200 mg N kg^{-1}, 47 mg P kg^{-1}, 377 mg K kg^{-1}, 64 mg S kg^{-1}, and 49 mg Mg kg^{-1}. Seven rhizoboxes were filled with 2.2 kg of dry soil per box to a height of 38 cm, resulting in a bulk density of 1.3 g cm^{-3}. Soil was rewetted from the bottom over a period of 112 h and pre-incubated in a climate chamber (Weiss-Umwelttechnik GmbH, Gießen, Germany) for 10 days. Conditions in the climate chamber during preincubation and the experiment were as follows: 16 h daylight with 300 μmol m^{-2} s^{-1} light intensity, 20 °C day temperature, 15 °C night temperature, 50 % relative humidity day, 60 % relative humidity night.

One rhizobox was equipped with two FDR sensors (ECH2O 5TE, Decagon Devices, Pullman, USA) at 5–10 cm and 30–35 cm depth measuring volumetric soil water content and soil temperature. Target soil moisture was 70 % WFPS to focus on root effects on denitrification and to ensure optimal conditions for O_2 optode and N_2O microsensor measurements. During the experiment, rhizoboxes were weighed and watered from the top every two-to-three days, always after N_2O flux measurements and O_2 imaging.

Maize seeds (*Zey mays* L. cv KWS Stabil) were pregerminated on wet paper for 3 days, and one germinated seed was planted into each box 10 days after rewetting the soil. However, plants emerged in only two rhizoboxes (3 and 4). From the remaining five rhizoboxes, old seeds were removed, and small maize seedlings of the same variety were planted. Measurements were conducted on the same days in relation to plant age (i.e., days after emergence) in all rhizoboxes to ensure comparability across replicates.

2.1.4. Harvest and soil sampling

The two rhizoboxes (Nr. 3 and 4), with initial seeds growing normally, were harvested 39 and 37 days after rewetting, corresponding to 25 and 21 days of plant growth, respectively. Rhizoboxes 1, 2, 5, 6, 7 with replanted seedlings were harvested 53, 49, 52, 50, and 52 days after rewetting, corresponding to 25, 21, 24, 22, and 24 days of plant growth. Due to the large workload of sampling and processing samples, it was not possible to harvest and sample all rhizoboxes on the same day. Shoots were cut above the surface and dried at 60 °C to determine shoot dry mass and N uptake.

In each rhizobox, regions of interest (ROI) were selected based on anoxic conditions (O_2 concentration < 10 % air saturation) and representing a range of root ages. Soil from ROI was sampled from the window side of the rhizoboxes with small aluminum cylinders (16 mm inner diameter, 10 mm depth, UGT Umwelt-Geräte-Technik GmbH, Müncheberg, Germany) and the roots were carefully separated from the soil. The soil was then homogenized and divided into three subsamples: ~1 g

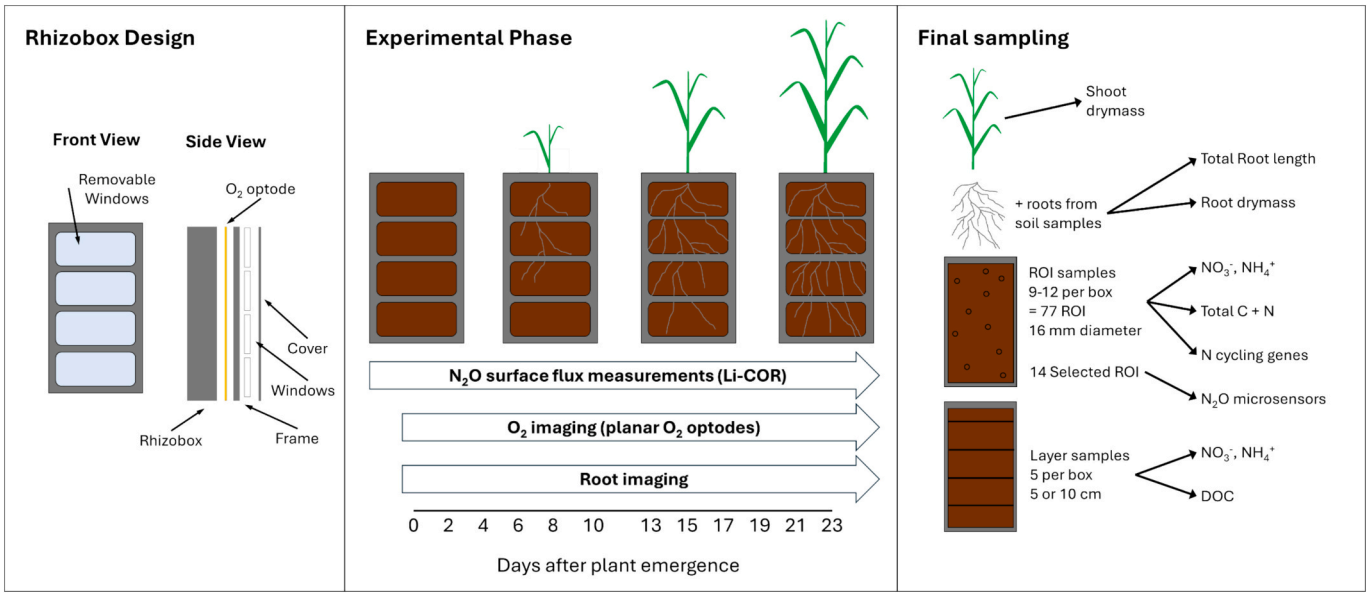

Fig. 1. Schematic overview of rhizobox design, experimental phase, and final sampling of the experiment. The rhizobox covers consisted of an opaque frame with 4 removable window panels. To monitor O_2 concentrations in soil, an O_2-sensitive optode was attached to the frame before closing the rhizoboxes.

soil (dry-weight-equivalent) was frozen in Eppendorf tubes (at –20 °C for analysis of bacterial functional genes, ~1 g soil (dry-weight-equivalent) was stored in 10 mL centrifuge tubes at 4 °C for analysis of mineral N, and the remaining soil (ca. 1–1.2 g) was dried at 105 °C to determine soil water content and total C and N content.

Additional soil samples were taken from rhizoboxes in 5 depths: 0–5 cm, 5–10 cm, 10–20 cm, 20–30 cm, 30–38 cm using a cork borer as auger (inner diameter 2 cm). For each depth layer, eight samples were taken from the window side of the rhizobox and homogenized into one composite sample, after careful removal of the roots. Each composite sample was then divided into three subsamples: ~50 g soil (dry-weight-equivalent) was stored at 4 °C for analysis of mineral N, ~10 g soil (dry-weight-equivalent) was stored at 4 °C for analysis of dissolved C_{org} (DOC), and ~ 5 g soil (dry-weight-equivalent) were dried at 105° C to determine soil water content.

Roots were washed from the remaining soil and stored in 30 % ethanol at 4 °C.

2.2. Oxygen and root imaging

2.2.1. Imaging setup

The imaging of the O_2 optodes was conducted with a single-lens reflex (SLR) camera (EOS 1300D, Canon, Japan) equipped with an objective lens (EFS 18–55 mm Canon, Japan), and an orange 530 nm long-pass filter (OG530 SCHOTT, 52 mm × 2 mm) with a plastic filter (#10 medium yellow, LEEfilters.com) attached in front of the long-pass filter to prevent autofluorescence of the long-pass filter. For excitation of the optode, a blue LED (470 nm, r-s components, Copenhagen, Denmark) was used. The LED was controlled by a USB-controlled LED driver unit (imaging.fish-n-chips.de). The software look@RGB (imaging.fish-n-chips.de) was used to gather the images and to control the camera and LED. Calibration of the O_2 optode was done as described in detail by Merl & Koren (2020). The O_2 imaging was conducted at two-to-three-day intervals, always on the same days as surface N_2O flux measurements.

Image processing and analysis were performed using the software ImageJ (imagej.nih.gov/ij/) using a ratiometric approach (Larsen et al., 2011; Merl & Koren, 2020). For the false-color images displaying O_2 concentration in % air saturation, the color palette *batlowK* (Scientific Color Maps v8.0.1, Crameri, 2018) was used. We calculated the anoxic area of the rhizobox window as the proportion of the image area with an O_2 concentration < 10 % air saturation (28.4 µmol O_2 L^{-1}) which is in the range of conditions promoting denitrification (Nakajima et al., 1984; Bonin et al., 1989) and similar to previous studies (Zhu et al., 2015; Keiluweit et al., 2018).

Prior to O_2 imaging, a photo of the rhizoboxes was taken with 'normal light conditions' to monitor root growth on the rhizobox window side. These root images were analyzed with RootPainter (Smith et al., 2022) to segment roots from the soil background. A model trained with randomly selected images was used to segment roots on all the images. Next, root length and root area were estimated from skeletonized images with RhizoVisionExplorer (Seethepalli et al., 2021). For image pre-processing, we used a thresholding level of 200, removed non-root objects that were smaller than 1 mm, an edge smoothing threshold of 2, and a pruning threshold of 5.

2.2.2. Post-harvest root scanning and analysis

Roots from each rhizobox were scanned on a flatbed scanner (Epson, Suwa, Japan) and the software RhizoVisionExplorer (Seethepalli et al., 2021) was used to extract total root length and total root volume from the scanned images. For image pre-processing, we used a thresholding level of 200, removed non-root objects that were smaller than 0.1 px, an edge smoothing threshold of 2, and a pruning threshold of 5. Root diameter classes were classified as < 1 mm, 1–2 mm, and > 2 mm. Total root dry weight was determined by drying roots at 105 °C. We refer to root length at the rhizobox window estimated with root imaging as *planar root length* and root length at the final harvest measured with root scanning as *total root length* (Wacker et al., 2024).

2.3. N_2O flux and microsensor measurements

2.3.1. N_2O surface flux analysis and calculations

Surface fluxes of N_2O emitted from soil were measured every two-to-three days using a N_2O/H_2O Trace Gas Analyzer (LI-7820, Li-COR, Lincoln, USA). Rhizoboxes were put into chambers consisting of an opaque bucket and a transparent chamber top. Chamber height was 50 cm, with a total volume of 36.2 L or adjusted to 150 cm (106.9 L) according to plant size. Chamber closing times were 4 and 10 min for small and large chambers, respectively. The temperature in the chamber was measured once at closing time and again before opening. The mean temperature was used for flux calculations. Nitrous oxide fluxes were calculated using the R package *goFlux* v0.2.0 (Rheault et al., 2024) and

cumulative N_2O emissions were calculated using *agg.fluxes* from the R package *gasfluxes* v0.6–2 (Fuß, 2020).

2.3.2. N_2O microsensor measurements

We used needle-shaped Clark-type N_2O microsensors that are based on an indium cathode in organic electrolyte and an O_2-removing compartment measuring N_2O partial pressures (Pa) in both gas and liquid (Andersen et al., 2001; Revsbech, 2021). Sensors were made inhouse, similar to those commercially available from Unisense (Unisense A/S, Aarhus, Denmark). The software SensorTrace Pro (Unisense A/S, Aarhus, Denmark) was used to introduce the sensor into the soil by a computer-controlled micromanipulator and to record the sensor signals. Calibration of the N_2O microsensors was performed in N_2O-free water and by addition of an N_2O-Standard (27 m*M* N_2O). All microsensors displayed a linear response curve during calibrations.

The N_2O microsensor measurements were conducted 23 days after plant emergence. In total, 14 regions of interest (ROI) in three different rhizoboxes (1, 4, 5) were chosen for N_2O microsensor measurements based on root development and O_2 concentration. Small holes (2 x 2 mm) were cut into the optode foil and N_2O depth profiles (0–5 mm, perpendicular to the optode) were measured in 500 µm steps. The number of measurements per ROI depended on variation in measured values, i.e., when two measurements showed similar low concentrations < 5 µmol N_2O L^{-1}, no further measurements were taken. For ROI with higher N_2O concentrations and/or high variability, up to six N_2O profiles were measured to capture heterogeneity within ROI.

2.4. Soil analysis, DNA extraction, and quantitative PCR

Soil mineral N was extracted by shaking the subsample with 1 *M* KCl (ratio 1:5 w:v) on an overhead shaker with 40 rpm for 60 min, filtered (Whatman Grade 42 for depth layer soil samples, 0.8 µm CA syringe filters for ROI samples), and analyzed colorimetrically on a continuous flow analyzer (AA3, Seal Analytical, Norderstedt, Germany). DOC was extracted by thoroughly shaking soil with ultrapure water (ratio 1:2 w:v) for 60 s, filtered through 0.45 µm PES syringe filters, and analyzed on an elemental analyzer (multi N/C 2100 S, Analytik Jena, Jena, Germany). Total C and N contents in ROI samples were analyzed on an elemental analyzer (Vario EL III, Elementar, Langenseibold, Germany).

Soil DNA was extracted from 400 mg of freeze-dried soil for each sample using the NucleoSpin Soil kit (Macherey-Nagel, Düren, Germany), following the manufacturer's instructions. The DNA quality was checked using a NanoDrop (Thermo Fisher Scientific, Waltham, MA, USA), before quantification on a Qubit fluorimeter using the Broad Range double stranded DNA kit (Thermo Fisher Scientific). The abundance of total archaea and bacteria (16S rRNA gene), denitrifiers (*nirK* and *nirS*), and N_2O reducers (*nosZ*I and *nosZ*II) were determined using real-time quantitative PCR (qPCR) using specific primers for each gene (Supplementary Table S1). The qPCR reactions were performed in two independent runs in a reaction volume of 15 µL containing iQ™ SYBR Green Supermix (Bio-Rad, Hercules, CA, USA), 0.1 % bovine serum albumin (New England Biolabs, Ipswich, MA, USA), primers, and 2 ng of template DNA on a CFX Connect Real-Time System (Bio-Rad). Primers, qPCR conditions, and amplification efficiencies are presented in Supplementary Table S1. Standard curves were generated by serial dilutions of linearized plasmids containing a fragment of the specific gene. The amplifications were validated by melting curve analyses and agarose gel electrophoreses. Potential inhibition of PCR reactions was initially checked by amplifying a known amount of the pGEM-T plasmid (Promega, Madison, WI, USA) with the plasmid specific M13F/M13R primer set (Supplementary Table S1) and 2 ng of DNA template or non-template controls for each sample. No inhibition was detected with the amount of DNA used.

2.5. Calculations and statistics

All calculations and statistics were carried out using the statistical software R v4.3.3 (R Core Team, 2024). Simple linear regressions were applied to identify relationships between soil moisture, planar root length, or anoxic soil area. Similarly, we applied simple linear regression models to analyze relationships between soil N_2O concentrations, O_2 concentrations, N availability, and abundance of N cycling genes in ROI at the end of the experiment. To identify the factors driving N_2O fluxes, we applied linear mixed effect models (lme) using the lme function from the package nlme v3.1–131 (Pinheiro et al., 2017). We tested models for the experimental period with and without plant growth, respectively, as well as for the whole experimental period. To account for repeated measurements, replicates were set as random effect. Models were compared using maximum likelihood (ML), selected using AIC (Akaike's information criterion), and fitted using restricted maximum likelihood (REML). Pseudo-R^2 for lme was calculated using r.squaredGLMM from the package MuMIn v1.42.1 (Barton, 2018).

3. Results

3.1. Plant and root growth

Root development followed the same pattern in all rhizoboxes. Planar root length increased slowly during the first week after emergence (146 ± 78 cm on day 8), then increased almost linearly until harvest (950 ± 444 cm, Fig. 2 a). Total root length at harvest was 161.4 ± 48.3 m, root dry weight was 1.11 ± 0.47 g, and root dry weight was positively correlated with total root length ($R^2 = 0.83$, $p < 0.01$). Maize shoot dry weight at harvest was 4.24 ± 1.16 g, and root:shoot ratio was 0.25 ± 0.03 (Supplementary Table S2). Shoot N content was 3.5 ± 0.4 %.

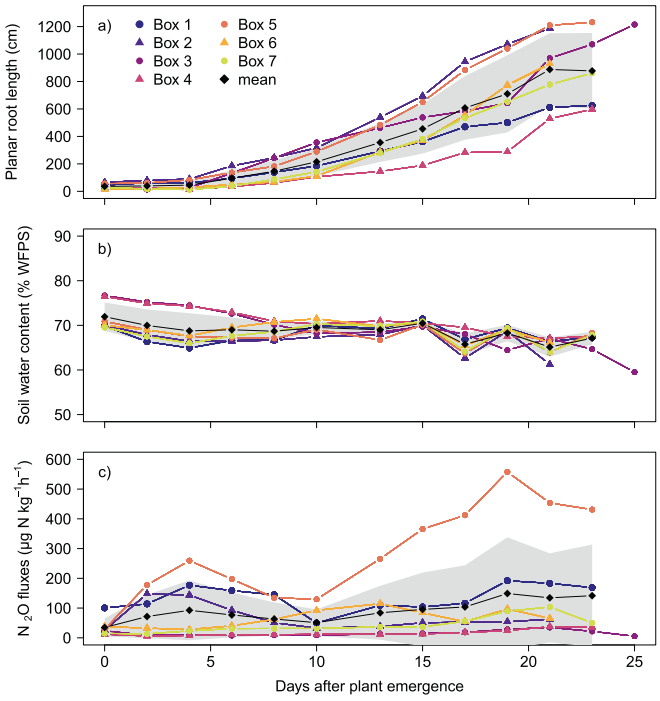

Fig. 2. (a) Planar root length (cm), (b) soil water content (% water-filled pore space), and (c) N_2O fluxes (µg N_2O-N $kg^{-1}h^{-1}$). Colored points and triangles represent each individual rhizobox, black diamonds and grey shaded area represent means ± standard deviation (n = 7).

3.2. Soil moisture

After rewetting, soil moisture ranged between 84 and 89 % WFPS (Supplementary Fig. S1) and was kept at 65–70 % WFPS during plant growth, providing favorable conditions for anaerobic processes such as denitrification (Fig. 2b). Soil moisture sensors showed that soil moisture was very stable in the 30–35 cm layer and fluctuated in the top 5–10 cm layer (Supplementary Fig. S2).

3.3. N_2O fluxes and cumulative emissions

The measured N_2O fluxes showed large variations between rhizoboxes with maximum N_2O fluxes ranging from 35 (Rhizobox 3) to 558 (Rhizobox 5) µg N_2O-N $kg^{-1}h^{-1}$ (Fig. 2c). During the acclimation phase, N_2O fluxes were comparable in all rhizoboxes and decreased during the first two weeks after rewetting (Supplementary Fig. S1). In the rhizoboxes that had to be replanted, N_2O fluxes remained relatively stable until plant emergence (Supplementary Fig. S1). In rhizoboxes 1, 2, and 5, N_2O fluxes increased directly after plant emergence, in rhizobox 6, N_2O fluxes increased slightly a week after plant emergence, and N_2O fluxes from rhizoboxes 1, 5, and 7 increased towards the end of the experiment (Fig. 2c). The N_2O fluxes from box 1 were higher than all other rhizoboxes before plant emergence (Supplementary Fig. S1), and highest from rhizobox 5 after plant emergence (Fig. 2c). Cumulative N_2O emissions during the planted phase averaged 48.8 ± 52.6 mg N_2O-N kg^{-1} (Supplementary Fig. S3).

3.4. Soil O_2 concentrations and anoxic soil fraction

Oxygen imaging was started 10 days after rewetting of the rhizoboxes, and most of the optode-soil interface was anoxic at this time (Example for Rhizobox 1 in Fig. 3, other data found in Supplementary Fig. S4 and S5). Overall, O_2 concentrations increased over time in all depths, although watering also led to formation of anoxic conditions in the upper soil layers without root growth (Fig. 3). In the deeper soil layers, the rhizobox window area covered with the O_2-sensitive planar optode showed almost completely anoxic conditions throughout the experiment. During plant growth, the anoxic fraction decreased in all layers in all rhizoboxes as the soil became increasingly more oxic. The O_2 concentrations rapidly increased in the topmost soil layer where >

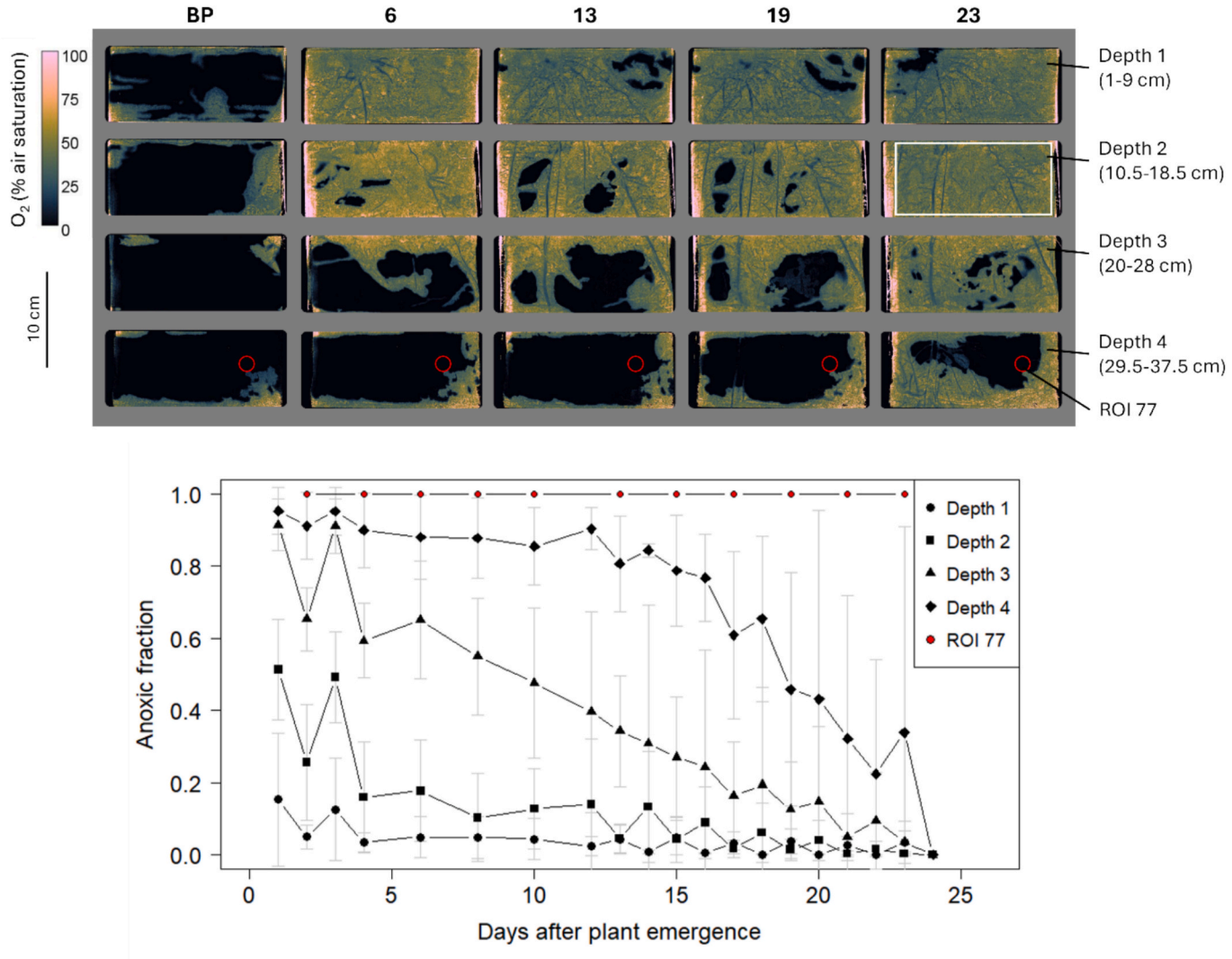

Fig. 3. Top: False color images of the O_2 concentrations in Rhizobox 1 before plant emergence (BP) and on Day 6, 13, 19, and 23 after plant emergence measured with planar O_2 optodes. The four 'windows' of the rhizobox correspond to the four depths. The white rectangle is exemplary for the area used to calculate the anoxic fraction of each depth. Lighter areas outside the white rectangle are artifacts at the edges of the optode and were not included in calculations. The red circle represents ROI 77.
Bottom: Fraction of anoxic area (< 10 % O_2 air saturation = 2.1 % O_2) in all rhizoboxes. Different symbols represent the four depths in the rhizoboxes and ROI 77. Mean ± standard deviation for n = 7.

90 % of the window area was oxic 24 days after plant emergence. Concentrations of O_2 in the depths below followed similar patterns, with a time delay. With increasing root growth, larger areas became oxic, but in the direct vicinity of roots, O_2 concentrations were lower compared to surrounding bulk soil.

3.5. Interactions between root growth, soil moisture, soil profile O_2 concentrations, and surface N_2O fluxes

Soil water content and mean anoxic fraction were both negatively correlated with root length (R^2 = 0.27 and 0.85, respectively, $p < 0.0001$), while the anoxic fraction was positively correlated with soil water content ($R^2 = 0.42$, $p < 0.0001$, Table 1, Supplementary Fig. S6). Linear regressions between surface N_2O fluxes and either soil water content, root length, or anoxic fraction yielded only weak relationships (Table 1, Supplementary Fig. S6).

The best model explaining surface N_2O fluxes included an interaction between soil water content and anoxic fraction as fixed factors and the rhizobox as random factor ($p < 0.01$). At a high anoxic fraction, ln(N_2O) was negatively correlated with soil water content. While for low anoxic fractions, ln(N_2O) was positively correlated with soil water content pointing towards interactive effects of soil water content and anoxia on N_2O formation and reduction. The conditional R^2 of the full model was 0.86, while the marginal R^2 of the model with only the fixed effect (i.e., without the random factor) was 0.09 highlighting the large differences between rhizoboxes (Table 1, Supplementary Fig. S7). Results of regression analyses for the dataset covering the whole experimental period can be found in the Supplementary Table S3.

3.6. Soil analyses (total CN, mineral N, DOC)

Soil analyses showed similar depth patterns for analysis of soil layers and ROI (Fig. 4). Soil NO_3^- content decreased with depth, from 706 ± 345 mg N kg^{-1} in the upper 5 cm to 246 ± 169 mg N kg^{-1} in the 5–10 cm layer to 26 ± 34 mg N kg^{-1} below 10 cm (Fig. 4a). Soil NH_4^+ contents in all ROI were lower than the amount of NH_4^+ added with fertilizer (52 mg NH_4^+-N kg^{-1}). The NH_4^+ contents were lowest in the 5–20 cm layers (1.0 ± 0.3 mg N kg^{-1}) and 4.8 ± 6.4 mg N kg^{-1} in the others (Fig. 4b). Total soil N in ROI was 0.14 ± 0.03 % without clear differences in different depths (Supplementary Fig. S8). Total soil C in ROI generally ranged between 1.11 and 1.25 % (1.19 ± 0.31 %) which was similar to the initial soil C_{org} content (1.21 %). From 77 measured ROI, eight ROI had higher total C contents between 1.5 and 2.3 % which likely included small pieces of roots or $CaCO_3$. The DOC content was 41.9 ± 31.4 mg C kg^{-1} with highest values in 0–5 cm layers (73.2 ± 57.6 mg C kg^{-1}, Fig. 4c).

Table 1
Results of regression analyses (coefficients of determination (Adjusted R^2), *p*-values, and sample size *n*) of the relationship between soil water content, root length, anoxic surface fraction, and N_2O surface fluxes (ln transformed) in rhizoboxes.

Response	Predictor	*n*	R^2	*p*-value
Simple linear regressions				
Soil water content	Planar root length	76	0.2738	7.42 x 10^{-07}
Anoxic fraction	Soil water content	76	0.4247	1.099 x 10^{-10}
Anoxic fraction	Planar root length	76	0.8482	< 2.2 x 10^{-16}
Root dry weight	Total root length	7	0.8303	0.002693
Soil water content	Total root length	7	0.8899	0.0008959
ln(N_2O)	Planar root length	76	0.06972	0.01263
ln(N_2O)	Soil water content	76	0.1058	0.002411
ln(N_2O)	Anoxic fraction	76	0.115	0.001593
Linear mixed effect model				
ln(N_2O)	Soil water content * Anoxic Fraction	76	0.857 (cond.)*	0.0097
	Random effect: Rhizobox Nr (replicate)		0.091 (marg.)*	

* For the linear mixed effect model (lme), the conditional R^2 is the variance explained by the entire model, including both fixed and random effects, while the marginal R^2 represents only the variance explained by the fixed effects.

3.7. Functional genes involved in N cycling

Abundance of 16S rRNA genes, a proxy for total archaea and bacteria, decreased with increasing sampling depth ($R^2 = 0.22$, $p < 0.0001$, Fig. 4d, Table 2). Similarly, abundance of *nirK* and *nosZ* clade II genes decreased with increasing sampling depth (R^2 = 0.39 and 0.47, respectively, $p < 0.0001$). For *nirS* and *nosZ* clade I, only very weak correlations with sampling depth were found (Table 2). Except for *nirS*, gene abundances were negatively correlated with soil NH_4^+ concentrations (Supplementary Table S4). However, NH_4^+ concentrations were also negatively correlated with soil depth. The ratio of denitrifiers (*nirK* + *nirS*) to N_2O reducers (*nosZ*I + *nosZ*II) increased with increasing NO_3^- content in ROI ($R^2 = 0.2$, $p < 0.0001$).

3.8. N_2O microsensor profiles in ROI and their relationship with influencing parameters

N_2O concentrations measured with N_2O microsensors in ROI at the end of the experiment showed very high variability in N_2O concentrations (Fig. 5, Supplementary Fig. S9). Concentrations of N_2O ranged between 0 and 100 µmol N_2O L^{-1} with the highest N_2O concentrations measured in ROI 1 close to the shoot and its crown roots at 1.1 cm depth and second highest measured in ROI 77 around a small root at the bottom of the rhizobox at 30.8 cm depth.

For most ROI, changes in N_2O concentration within the same measurement profile were in the range of a few µmol (Supplementary Fig. S9). There were exceptions, such as ROI 1 where one N_2O profile increased from 20 to 100 µmol L^{-1} and ROI 77 where N_2O concentrations increased from 0 to 40–60 µmol L^{-1} in 2–5 mm depth (Fig. 5). In the direct proximity of the optode (500 µm depth), minimum N_2O concentrations were negatively correlated with maximum O_2 concentration ($R^2 = 0.53$, $p < 0.01$, Table 2, Supplementary Fig. S10), while maximum N_2O concentrations in 500 µm depth were positively correlated with total N availability in all ROI ($R^2 = 0.52$, $p < 0.01$, Table 2, Supplementary Fig. S10).

4. Discussion

4.1. Microsite N_2O formation depended on root growth, O_2 and N availability

Nitrous oxide microsensor measurements revealed a very high spatial heterogeneity of N_2O formation in the rhizobox soils. The fact that minimum N_2O concentrations were higher in ROI with lower O_2 concentrations confirms that O_2 availability was a major control of denitrification at the microscale. Oxygen concentration is one of the most important controls of denitrification as it determines when microorganisms switch to anaerobic respiration (Groffman et al., 1988; Schlüter et al., 2024). This, however, does not ascertain that denitrification will occur, as nitrate can be limiting (Smith & Tiedje, 1979; Hojberg et al., 1994; Schlüter et al., 2024), which has been documented in relation to plant growth with rapid N uptake (von Rheinbaben & Trolldenier, 1984; Haider et al., 1985; Rummel et al., 2021). Accordingly, we found higher N_2O concentrations in ROI with higher total N availability indicating that, under O_2 limiting conditions, N availability is crucial to determine the magnitude of N_2O emissions. The ROI with the highest N_2O concentrations were in the direct vicinity of roots (i.e., ROI Nr. 1, 77), confirming the stimulating effect of roots on

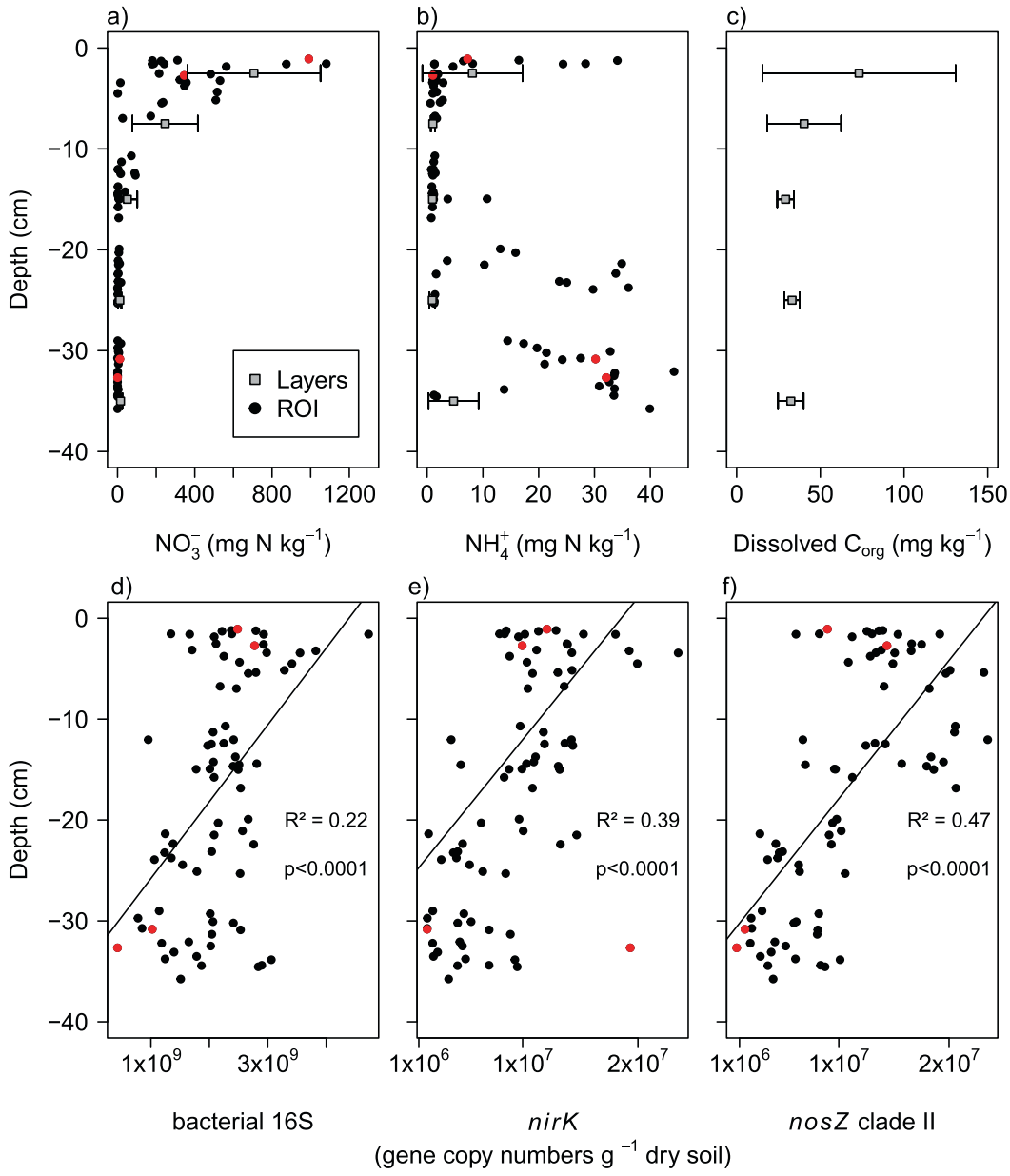

Fig. 4. Depth distribution of (a) NO_3^-, (b) NH_4^+, and (c) DOC content in soil layers and ROI, and (d-f) depth distribution of gene abundances in ROI. Each point represents one of 77 ROI, while grey squares represent mean values ± standard deviation (n = 7) for different soil layers. Red circles represent ROI Nr. 1, 6, 45, and 77. For gene abundances, regression lines, adjusted R^2, and *p*-values of simple linear regressions with depth are depicted.

denitrification. ROI 45 was characterized by high NO_3^- content and anoxic conditions, but no roots, and only low N_2O concentrations confirming the importance of roots on formation of N_2O hotspots through C exudation, root and rhizosphere microbial respiration. Continuous anoxia, root growth, and high abundance of denitrifiers (*nirK* + *nirS*) could indicate a hotspot in ROI 6, yet the low N_2O concentrations combined with low availability of NO_3^-, and very low abundance of N_2O reducers (*nosZ*I + *nosZ*II) contradict this. Although functional gene abundances and N_2O concentrations were not significantly correlated in ROI, we found a positive relationship between the (*nirK* + *nirS*)/(*nosZ*I + *nosZ*II) ratio and NO_3^- availability suggesting higher relative genetic potential for N_2O reduction at lower soil NO_3^- content. This relationship was driven by the abundance of *nosZ* clade II nitrous oxide reducers, in line with previous reports (Xu et al., 2020; Jones et al., 2022). To fully elucidate N_2O reduction dynamics, measurements of N_2O reduction enzyme activity, expression of functional genes related to N_2O reduction, or direct measurements of N_2O reduction rates should be included in future studies.

4.2. Roots determined biotic and abiotic gradients in soil

Plant and root growth affected soil moisture, anoxic soil fraction, and distribution of nutrients controlling the abundance of microorganisms. Root growth determined soil moisture through root water uptake as demonstrated by significant negative correlations between soil water content and planar root length throughout the experiment and between soil water content and total root length at final harvest. Further, soil moisture sensors showed that soil moisture was constant at the bottom of the rhizoboxes, while fluctuating more in the upper soil layer with higher root density. Using planar optodes, we were able to show increasing O_2 concentrations with increasing plant and root growth. Especially, roots growing into deeper soil layers led to increasing O_2 concentrations at the optode-soil interface. We anticipate a combination of several explanations: (1) plant roots can increase the diffusion of O_2

Table 2
Results of simple linear regression analyses (coefficients of determination (Adjusted R^2), *p*-values, and sample size *n*) of the relationship between N_2O, O_2, mineral N concentrations, root age, soil depth, and abundance of N cycling genes in ROI.

Response	Predictor	*n*	R^2	*p*-value
Min. N_2O concentration	Max. O_2 concentration	14	0.5304	0.001893
Max. N_2O concentration	N concentration	14	0.5227	0.002097
16S abundance	Depth	77	0.2193	1.04×10^{-05}
nirK abundance	Depth	77	0.3882	8.65×10^{-10}
nirS abundance	Depth	77	0.04388	0.03745
*nosZ*I abundance	Depth	77	0.07119	0.01085
*nosZ*II abundance	Depth	77	0.4691	3.891×10^{-12}
NH_4^+ content	Depth	77	0.3325	2.436×10^{-08}
nirK abundance	Root age	77	0.2431	3.127×10^{-06}
*nosZ*II abundance	Root age	77	0.1822	6.433×10^{-05}
(*nirK* + *nirS*) / (*nosZ*I + *nosZ*II)	NO_3^- content	76	0.2	3.045×10^{-05}

through the soil (Jensen & Kirkham, 1963), (2) maize roots form aerenchyma under O_2-limited conditions ($\leq$ 3 % O_2 $\approx$ 14.3 % O_2 air saturation, Gunawardena et al., 2001) facilitating transport of O_2 into anoxic soil layers, (3) and roots may have 'pushed' the optode away from the soil surface in some spots creating air-filled cavities between the optode and the soil (Merl et al., 2023). Although roots generally increased aeration and O_2 concentrations in soil, roots were always characterized by lower O_2 concentrations compared to the surrounding soil, confirming the formation of anoxic microsites in the rhizosphere under our experimental conditions (Lacroix et al., 2025).

Most of the added N fertilizer was recovered as NO_3^- in the upper 10 cm of the rhizoboxes, likely due to a combination of initial rewetting the soil in the rhizoboxes from the bottom and evaporation on the soil surface causing a constant upward movement of soil water, transporting NO_3^- to the upper soil layer throughout the experiment. Total mineral N recovery in soil and NH_4^+ concentrations were always lower than the amount of added fertilizer confirming that N reduction and immobilization were dominant processes in our study.

Root growth increased availability of organic C through rhizodeposition leading to higher DOC concentrations in upper soil layers with higher root density. Although root exudation per root surface area decreases with growth/age, total exuded C rates increase with increasing root growth (Santangeli et al., 2024). Especially, maize crown/brace roots can exude large quantities of mucilage containing high amounts of sugars (Werner et al., 2022) contributing to high availability of DOC in the uppermost soil layers. Higher availability of DOC and NO_3^- in upper soil layers promoted microbial growth as indicated by decreasing abundances of 16S rRNA, *nirK* and *nosZ*II genes with soil depth. Abundances of *nirK* and *nosZ*II genes also increased with increasing root age confirming the influence of root growth on microbial denitrifiers. Abundances of *nirS* and *nosZI* were much lower compared to abundances of *nirK* and *nosZII*, respectively, and were not affected by nutrient concentrations or root growth indicating niche differentiation between *nirK*- and *nirS*-type denitrifiers and *nosZ* clade I and II nitrous oxide reducers, respectively (Jones & Hallin, 2010; Achouak et al., 2019; Wang et al., 2024).

4.3. Soil moisture and anoxic fraction controlled N_2O fluxes

The N_2O fluxes showed distinct patterns with initially high fluxes decreasing until about two weeks after rewetting the soil, followed by a period with lower fluxes. Emergence of plants stimulated N_2O production leading to clear increases in N_2O fluxes within a week following plant emergence. However, correlations between N_2O fluxes and planar root length or cumulative N_2O emissions and total root length at harvest did not yield significant relationships as we would have expected. Nonetheless, our study confirmed intercorrelation of root growth and N_2O formation as N_2O fluxes were controlled by an interaction of the anoxic fraction and soil moisture, confirming interacting effects of root water uptake and anaerobicity on N_2O formation and reduction. For low anoxic fractions, increasing soil moisture led to increasing N_2O fluxes, while for high anoxic fractions higher soil moisture led to lower N_2O fluxes due to the reduction of N_2O to N_2 (Davidson, 1991; Rohe et al., 2021).

In addition, differences between replicates explained most of the variance in N_2O fluxes. Soil heterogeneity is known to strongly control the formation of denitrifying N_2O hotspots causing very high variation within replicates of the same treatment (Folorunso & Rolston, 1984;

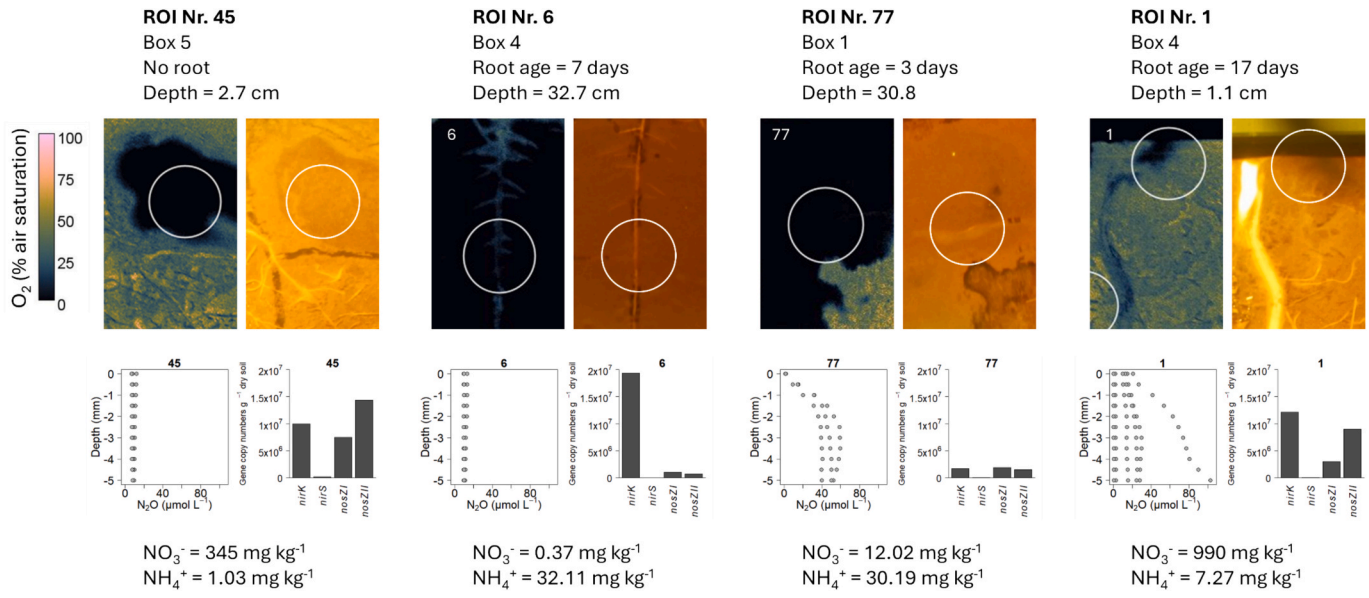

Fig. 5. Characterization of four exemplary ROI at the end of the experiment. False-color image showing O_2 concentration, photo showing root development, N_2O microsensor profiles (µmol N_2O, depth representing the distance from the optode), bar plot showing gene abundances (gene copy numbers g^{-1} dry soil), and mineral N content (mg N kg^{-1}). ROI diameter = 16 mm. Root age refers to the days of root growth in the respective ROI.

Christensen et al., 1990; Schlüter et al., 2024). Plant and root growth further increased heterogeneity in soil but also differences between replicates.

4.4. The uppermost soil layers contributed largely to N_2O fluxes

Our results indicate that some zones of the rhizoboxes were more likely to contribute to N_2O formation – the uppermost and the lowermost soil layers. The upper 5 cm soil layer was characterized by very high NO_3^- concentrations (up to > 1000 mg NO_3^--N kg^{-1}), highest concentrations of DOC, and highest abundances of denitrifying and N_2O reducing genes (*nirK* and *nosZ*II). Although O_2 concentrations in the uppermost soil layer increased fast, small anoxic areas were identified with the O_2 optodes at the later/last measurement days. Furthermore, rewatering from the top kept soil continuously wet which (together with high NO_3^- and DOC) provided optimal conditions for denitrifiers as confirmed by microsensor measurements (ROI 1). Short distance to the soil surface facilitated N_2O diffusion to the surface and its loss to the atmosphere. Accordingly, cumulative N_2O emissions were positively correlated with soil NO_3^- content in the uppermost soil layer. By contrast, the bottom layer of the rhizoboxes had larger areas that remained anoxic throughout the experiment. Here, the NO_3^- concentrations in the bottom layer were low (15 mg NO_3^--N kg^{-1}, 200 μM NO_3^-), but sufficient to sustain denitrifying microorganisms (Palmer & Horn, 2015) as confirmed by N_2O microsensor profiles indicating substantial N_2O formation around a small root in ROI 77. Continuous high soil moisture and long diffusion pathways from the lower soil layers of the rhizobox to the soil surface likely promoted N_2O reduction to N_2.

5. Conclusions

We provide the first *in-situ* measurements of N_2O concentration profiles showing distinct patterns with highest N_2O concentrations around roots compared to bulk soil. Our study confirmed that O_2 and N availability control N_2O production at the process scale while emphasizing the importance of roots in shaping N_2O hotspots. Plant roots determined depth gradients with higher DOC and lower soil moisture in the upper soil layers of the rhizoboxes. Bacteria, denitrifying *nirK* and N_2O reducing *nosZ*II responded to resource availability with higher abundances in the upper soil layers, that had high nutrient contents and a more pronounced root growth. Our results suggest that these uppermost soil layers largely contributed to N_2O formation and thus the N_2O fluxes measured at the soil surface. Combining O_2 optode and root imaging proved to be a successful approach to monitor major controls of rhizosphere N cycling and N_2O formation at high spatial and temporal resolution. Carefully choosing ROIs allowed reducing the number of samples, while covering a broad range of soil conditions revealing correlations between N_2O concentrations, substrate availability, and microbial gene abundances. Future studies should focus on elucidating dynamics of N_2O formation in hotspots in relation to aboveground N_2O fluxes. For soils with lower moisture and coarser texture, other processes contributing to N_2O formation (nitrification, nitrifier-denitrification) also need to be addressed.

CRediT authorship contribution statement

Pauline Sophie Rummel: Writing – original draft, Investigation, Data curation, Conceptualization. **Martin Reinhard Rasmussen:** Writing – review & editing, Investigation. **Aurélien Saghaï:** Writing – review & editing, Investigation, Data curation. **Theresa Merl:** Writing – review & editing, Data curation. **Sara Hallin:** Writing – review & editing. **Carsten W. Mueller:** Writing – review & editing, Conceptualization. **Klaus Koren:** Writing – review & editing, Conceptualization.

Declaration of competing interest

The authors declare the following financial interests/personal relationships which may be considered as potential competing interests: Pauline Sophie Rummel reports financial support was provided by Novo Nordisk Foundation. Martin Reinhard Rasmussen reports financial support was provided by Danish National Research Foundation. Given their role as Chief Editor for Special Issues and Reviews, Carsten W. Mueller had no involvement in the peer-review of this article and has no access to information regarding its peer-review. Full responsibility for the editorial process for this article was delegated to another journal editor. If there are other authors, they declare that they have no known competing financial interests or personal relationships that could have appeared to influence the work reported in this paper.

Acknowledgements

The authors would like to thank Lars Borregaard Pedersen at AU for excellent technical support, Tomke S. Wacker, Frederik van der Bom, and Lorène Siegwart at KU for support on root imaging, scanning, and analysis, Andrey Kalinichev and Fabian Steininger at AU for help with optode calibration, Sabine Rautenberg and Claudia Kuntz at TU Berlin for soil analyses, Franziska Eller at AU for access to the climate chambers and LiCOR, and Per Lennart Ambus and Kristian Thorup-Kristensen at KU for feedback on the experimental setup.

Funding

PSR was supported by a Novo Nordisk Fonden (NNF) Postdoctoral Fellowship (grant number NNF22OC0079335). MRR was supported by the Pioneer Center for Research in Sustainable Agricultural Futures (Land-CRAFT), DNRF grant number P2.

Appendix A. Supplementary data

Supplementary data to this article can be found online at https://doi.org/10.1016/j.geoderma.2026.117734.

Data availability

The data that support the findings of this study will be made openly available at http://doi.org/10.5281/zenodo.15537545.

References

Achouak, W., Abrouk, D., Guyonnet, J., Barakat, M., Ortet, P., Simon, L., Lerondelle, C., Heulin, T., El Zahar, H.F., 2019. Plant hosts control microbial denitrification activity. FEMS Microbiol. Ecol. 95, 1–13.

Ai, C., Zhang, M., Sun, Y., Zhang, L., Zeng, L., Liu, Y., Wang, X., Chai, Y., He, P., Liang, G., et al., 2020. Wheat rhizodeposition stimulates soil nitrous oxide emission and denitrifiers harboring the nosZ clade I gene. Soil Biol. Biochem. 143.

Andersen, K., Kjar, T., Revsbech, N.P., 2001. An oxygen insensitive microsensor for nitrous oxide. Sens. Actuators B 81, 42–48.

Bakken LR. 1988. Denitrification under different cultivated plants: effects of soil moisture tension, nitrate concentration, and photosynthetic activity. **6**: 271–278.

Barton K. 2018. MuMIn: Multi-Model Inference.

Bateman, E.J., Baggs, E.M., 2005. Contributions of nitrification and denitrification to N2O emissions from soils at different water-filled pore space. Biol. Fertil. Soils 41, 379–388.

Ben-Noah, I., Friedman, S.P., 2018. Review and evaluation of root respiration and of natural and agricultural processes of soil aeration. Vadose Zone J. 17, 170119.

Blossfeld, S., 2013. Light for the dark side of plant life: -Planar optodes visualizing rhizosphere processes. Plant and Soil 369, 29–32.

Bonin, P., Gilewicz, M., Bertrand, J.C., 1989. Effects of oxygen on each step of denitrification on *Pseudomonas nautica*. Can. J. Microbiol. 35, 1061–1064.

Butterbach-Bahl, K., Baggs, E.M., Dannenmann, M., Kiese, R., Zechmeister-Boltenstern, S., 2013. Nitrous oxide emissions from soils: how well do we understand the processes and their controls? Philos. Trans. R. Soc. B 368, 1–13.

Chèneby, D., Perrez, S., Devroe, C., Hallet, S., Couton, Y., Bizouard, F., Iuretig, G., Germon, J.C., Philippot, L., 2004. Denitrifying bacteria in bulk and maize-rhizospheric soil: diversity and N $_2$ O-reducing abilities. Can. J. Microbiol. 50, 469–474.

Christensen, S., Groffman, P., Mosier, A., Zak, D.R., 1990. Rhizosphere denitrification; a minor process but indicator of decomposition activity. In: In: Denitrification in Soil and Sediment, pp. 199–211.
Ciais, P., Sabine, C., Bala, G., Bopp, L., Brovkin, V., Canadell, J., Chhabra, A., DeFries, R., Galloway, J., Heimann, M., et al., 2013. Carbon and other biogeochemical cycles. In: Climate Change 2013: the Physical Science Basis. Contribution of Working Group I to the Fifth Assessment Report of the Intergovernmental Panel on Climate Change, pp. 465–570.
Crameri F. 2018. Scientific Colour Maps.
Davidson, E.A., 1991. Fluxes of nitrous oxide and nitric oxide from terrestrial ecosystems. In: Rogers, J.E., Whitman, W.B. (Eds.), Microbial Production and Consumption of Greenhouse Gases: Methane, Nitrogen Oxides and Halomethanes. American Society for Microbiology, Washington (DC), pp. 219–235.
Folorunso, O.A., Rolston, D.E., 1984. Spatial variability of field-measured denitrification gas fluxes. Soil Sci. Soc. Am. J. 48, 1214–1219.
Fuß R. 2020. gasfluxes: Greenhouse Gas Flux Calculation from Chamber Measurements.
Groffman, P.M., Butterbach-Bahl, K., Fulweiler, R.W., Gold, A.J., Morse, J.L., Stander, E. K., Tague, C., Tonitto, C., Vidon, P., 2009. Challenges to incorporating spatially and temporally explicit phenomena (hotspots and hot moments) in denitrification models. Biogeochemistry 93, 49–77.
Groffman PM, Tiedje JM, Robertson GP, Christensen S. 1988. Denitrification at different temporal and geographical scales: Proximal and distal controls. In: Wilson JR, ed. Advances in Nitrogen Cycling in Agricultural Ecosystems. 174–192.
Gunawardena, A.H.L.A.N., Pearce, D.M.E., Jackson, M.B., Hawes, C.R., Evans, D.E., 2001. Rapid changes in cell wall pectic polysaccharides are closely associated with early stages of aerenchyma formation, a spatially localized form of programmed cell death in roots of maize (*Zea mays* L.) promoted by ethylene. Plant Cell Environ. 24, 1369–1375.
Guyonnet, J.P., Vautrin, F., Meiffren, G., Labois, C., Cantarel, A.A.M., Michalet, S., Comte, G., Haichar, F.el.Z., 2017. The effects of plant nutritional strategy on soil microbial denitrification activity through rhizosphere primary metabolites. FEMS Microbiol. Ecol. 93, 1–11.
Haider, K., Mosier, A., Heinemeyer, O., 1985. Phytotron experiments to evaluate the effect of growing plants on denitrification. Soil Sci. Soc. Am. J. 49, 636–641.
Hamonts, K., Clough, T.J., Stewart, A., Clinton, P.W., Richardson, A.E., Wakelin, S.A., O'Callaghan, M., Condron, L.M., 2013. Effect of nitrogen and waterlogging on denitrifier gene abundance, community structure and activity in the rhizosphere of wheat. FEMS Microbiol. Ecol. 83, 568–584.
Hojberg, O., Revsbech, N.P., Tiedje, J.M., 1994. Denitrification in soil aggregates analyzed with microsensors for nitrous oxide and oxygen. Soil Sci. Soc. Am. J. 58, 1691–1698.
Hu, H.W., Chen, D., He, J.Z., 2015. Microbial regulation of terrestrial nitrous oxide formation: understanding the biological pathways for prediction of emission rates. FEMS Microbiol. Rev. 39, 729–749.
Jensen, C.R., Kirkham, D., 1963. Labeled Oxygen: Increased Diffusion Rate through Soil Containing Growing Corn Roots. Science 141 (3582), 735–736. http://www.jstor.org/stable/1710795.
Jones, C.M., Hallin, S., 2010. Ecological and evolutionary factors underlying global and local assembly of denitrifier communities. ISME J. 4, 633–641.
Jones, C.M., Putz, M., Tiemann, M., Hallin, S., 2022. Reactive nitrogen restructures and weakens microbial controls of soil N2O emissions. Commun. Biol. 5.
Keiluweit, M., Gee, K., Denney, A., Fendorf, S., 2018. Anoxic microsites in upland soils dominantly controlled by clay content. Soil Biol. Biochem. 118, 42–50.
Klemedtsson, L., Svensson, B.H., Rosswall, T., 1987. Dinitrogen and nitrous oxide produced by denitrification and nitrification in soil with and without barley plants. Plant and Soil 99, 303–319.
Knowles, R., 1982. Denitrification. Microbiolagical Reviews 46, 43–70.
Kuzyakov, Y., Blagodatskaya, E.V., 2015. Microbial hotspots and hot moments in soil: Concept & review. Soil Biol. Biochem. 83, 184–199.
Lacroix, A.M., Frei, J., van der Loo, E., Kocsis, L., Keiluweit, M., 2025. Root exudation and fine texture interact to form anoxic microsites in rhizosphere soil. Soil Biol. Biochem. 211, 109974.
Lambers, H., Mougel, C., Jaillaird, T., Hinsinger, P., 2009. Plant-microbe-soil interactions in the rhizosphere: an evolutionary perspective. Plant and Soil 321, 83–115.
Larsen, M., Borisov, S.M., Grunwald, B., Klimant, I., Glud, R.N., 2011. A simple and inexpensive high resolution color ratiometric planar optode imaging approach: application to oxygen and pH sensing. Limnol. Oceanogr. Methods 9, 348–360.
Mahmood, T., Ali, R., Malik, K.A., Shamsi, S.R.A., 1997. Denitrification with and without plant (*Zea mays* L.) under irrigated field conditions. Biol Fert Soils 24, 323–328.
Malique, F., Ke, P., Boettcher, J., Dannenmann, M., Butterbach-Bahl, K., 2019. Plant and soil effects on denitrification potential in agricultural soils. Plant and Soil 439, 459–474.
Merl, T., Hu, Y., Pedersen, J., Zieger, S.E., Bornø, M.L., Tariq, A., Sommer, S.G., Koren, K., 2023. Optical chemical sensors for soil analysis: possibilities and challenges of visualizing NH3 concentrations as well as pH and O2 microscale heterogeneity. Environ. Sci.: Adv. 00, 1–10.
Merl, T., Koren, K., 2020. Visualizing NH3 emission and the local O2 and pH microenvironment of soil upon manure application using optical sensors. Environ. Int. 144, 106080.
Nakajima, M., Hayamizu, T., Nishimura, H., 1984. Effect of oxygen concentration on the rates of denitratification and denitrification in the sediments of an eutrophic lake. Water Res. 18, 335–338.
Palmer, K., Horn, M.A., 2015. Denitrification activity of a remarkably diverse fen denitrifier community in finnish Lapland is N-oxide limited. PLoS One 10.
Pausch, J., Kuzyakov, Y., 2018. Carbon input by roots into the soil: Quantification of rhizodeposition from root to ecosystem scale. Glob. Chang. Biol. 24, 1–12.
Philippot, L., Hallin, S., Börjesson, G., Baggs, E.M., 2009. Biochemical cycling in the rhizosphere having an impact on global change. Plant and Soil 321, 61–81.
Philippot, L., Raaijmakers, J.M., Lemanceau, P., Van Der Putten, W.H., 2013. Going back to the roots: the microbial ecology of the rhizosphere. Nat. Rev. Microbiol. 11, 789–799.
Pinheiro J, Bates D, DebRoy S, Sarkar D, R Core Team. 2017. nlme: Linear and Nonlinear Mixed Effects Models.
R Core Team. 2024. R: A Language and Environment for Statistical Computing.
Revsbech, N.P., 2021. Simple sensors that work in diverse natural environments: the micro-Clark sensor and biosensor family. Sens. Actuators B 329, 129168.
Rheault, K., Christiansen, J.R., Larsen, K.S., 2024. goFlux: a user-friendly way to calculate GHG fluxes yourself, regardless of user experience. Journal of Open Source Software 9, 6393.
von Rheinbaben, W., Trolldenier, G., 1984. Influence of plant growth on denitrification in relation to soil moisture and potassium nutrition. Zeitschrift Für Pflanzenernärung Und Bodenkunde 147, 730–738.
Rohe, L., Apelt, B., Vogel, H.-J., Well, R., Wu, G.-M., Schlüter, S., 2021. Denitrification in soil as a function of oxygen availability at the microscale. Biogeosciences 18, 1185–1201.
Rummel, P.S., Well, R., Pfeiffer, B., Dittert, K., Floßmann, S., Pausch, J., 2021. Nitrate uptake and carbon exudation – do plant roots stimulate or inhibit denitrification? Plant and Soil 459, 217–233.
Santangeli, M., Steininger-Mairinger, T., Vetterlein, D., Hann, S., Oburger, E., 2024. Maize (*Zea mays* L.) root exudation profiles change in quality and quantity during plant development – A field study. Plant Science 338, 111896.
Schlüter, S., Lucas, M., Grosz, B., Ippisch, O., Zawallich, J., He, H., Dechow, R., Kraus, D., Blagodatsky, S., Senbayram, M., et al., 2024. The anaerobic soil volume as a controlling factor of denitrification: a review. Biol. Fertil. Soils.
Seethepalli, A., Dhakal, K., Griffiths, M., Guo, H., Freschet, G.T., York, L.M., 2021. RhizoVision Explorer: Open-source software for root image analysis and measurement standardization. AoB Plants 13, 1–15.
Senbayram, M., Well, R., Shan, J., Bol, R., Burkart, S., Jones, D.L., Wu, D., 2020. Rhizosphere processes in nitrate-rich barley soil tripled both N2O and N2 losses due to enhanced bacterial and fungal denitrification. Plant and Soil 448, 509–522.
Smith, A.G., Han, E., Petersen, J., Olsen, N.A.F., Giese, C., Athmann, M., Dresbøll, D.B., Thorup-Kristensen, K., 2022. R oot P ainter : deep learning segmentation of biological images with corrective annotation. New Phytol. 236, 774–791.
Smith, M.S., Tiedje, J.M., 1979. Phases of denitrification following oxygen depletion in soil. Soil Biol. Biochem. 11, 261–267.
Starkey, R.L., 1958. Interrelations between microorganisms and plant roots in the rhizosphere. Bacteriol. Rev. 22, 154–172.
IUSS Working Group WRB. 2022. World Reference Base for Soil Resources, 4th edn. International Union of Soil Sciences (IUSS), Vienna, Austria.
Vinther, F.P., 1984. Total denitrification and the ratio between N2O and N2 during the growth of spring barley. Plant and Soil 76, 227–232.
Wacker, T.S., van der Bom, F., Delory, B.M., Vetterlein, D., Postma, J.A., Nagel, K.A., Schnepf, A., Dresbøll, D.B., 2024. Back to the roots: standardizing root length density terminology. Plant and Soil.
Wang, J., Zhang, Z., Liang, F., Che, Z., Wen, Y., Zhang, M., Jin, W., Dong, Z., Song, H., 2024. Decreased soil pH weakens the positive rhizosphere effect on denitrification capacity. Pedosphere 34, 905–915.
Werner, L.M., Knott, M., Diehl, D., Ahmed, M.A., Banfield, C., Dippold, M., Vetterlein, D., Wimmer, M.A., 2022. Physico-chemical properties of maize (*Zea mays* L.) mucilage differ with the collection system and corresponding root type and developmental stage of the plant. Plant and Soil 478, 103–117.
Woldendorp, W., 1963. The Influence of living Plants on Denitrification. Meded Landbouwhogeschool Wageningen 63, 1–100.
Xu, X., Liu, Y., Singh, B.P., Yang, Q., Zhang, Q., Wang, H., Xia, Z., Di, H., Singh, B.K., Xu, J., et al., 2020. *NosZ* clade II rather than clade I determine *in situ* N2O emissions with different fertilizer types under simulated climate change and its legacy. Soil Biol. Biochem. 150, 107974.
Yankelzon, I., Willibald, G., Dannenmann, M., Malique, F., Ostler, U., Scheer, C., Butterbach-Bahl, K., 2024. A new incubation system to simultaneously measure n2 as well as n2o and co2 fluxes from plant-soil mesocosms. Biol. Fertil. Soils.
Zhao, S., Zhou, J., Yuan, D., Wang, W., Zhou, L., Pi, Y., Zhu, G., 2020. NirS-type N2O-producers and nosZ II-type N2O-reducers determine the N2O emission potential in farmland rhizosphere soils. J. Soil. Sediment. 20, 461–471.
Zhu, K., Bruun, S., Larsen, M., Glud, R.N., Jensen, L.S., 2015. Heterogeneity of O2 dynamics in soil amended with animal manure and implications for greenhouse gas emissions. Soil Biol. Biochem. 84, 96–106.
Zumft, W.G., 1997. Cell biology and molecular basis of denitrification. Microbiol Mol Biol Rev 61, 533–616.